Journal of MATERIALS RESEARCH

Article
DOI:10.1557/s43578-022-00535-z

TRANSITION METAL-BASED NANOMATERIALS

FOCUS ISSUE

Electrochemical energy storage on nanoporous copper sponge

David J. McPherson[1], Annette Dowd[1], Matthew D. Arnold[1], Angus Gentle[1], Michael B. Cortie[1,a)]

[1] School of Mathematical and Physical Sciences, University of Technology Sydney, PO Box 123, Broadway, NSW 2007, Australia
[a)] Address all correspondence to this author. e-mail: michael.cortie@gmail.com

Received: 27 November 2021; accepted: 1 March 2022; published online: 14 March 2022

A proof-of-principle double-layer symmetrical supercapacitor with nanoporous copper/copper oxide electrodes and an aqueous electrolyte is investigated. The electrodes are manufactured by selective dissolution of Al from a eutectic composition of $Cu_{17.5}Al_{82.5}$ using 5 M NaOH. The ostensible (i.e., net external) capacitance of a symmetrical two-electrode cell with 0.1 M KNO_3 electrolyte is assessed over a series of charge/discharge cycles and is about 2 F per gram of Cu in this simple prototype. Capacitance varies during a discharge cycle due evidently to the deeply buried surfaces and pseudocapacitive reactions contributing charge toward the end of a discharge cycle. In principle such a device should have very low ohmic losses due to its highly conductive backbone and would be suitable for applications requiring maximum energy efficiency over repeated cycling. The aqueous electrolyte ensures fire safety but this comes at the cost of lower energy content.

Introduction

Temporary storage is a key requirement in the effective utilization of electrical energy, and this need is generally met by batteries and capacitors of various kinds [1–3]. Supercapacitors, which exploit electrochemical double-layer capacitance (DLC) and, sometimes, electrochemical pseudocapacitance, have attracted considerable attention as they can store and release electrical energy at high power density and moderate energy density [3–6]. (The term pseudocapacitance refers to devices in which some charge is stored and released from an electrode's surface via chemical rather than purely physical capacitive processes.) As such, the characteristics exhibited by supercapacitors bridge the gap in power and energy density between conventional capacitors and batteries. Consequently, supercapacitors may be used in such applications as communication and aviation, portable electronics, energy recovery in electric or hybrid vehicles, uninterruptable power supplies, or to stabilize fluctuating loads in photovoltaic devices. In general these supercapacitors are almost exclusively based on carbonaceous electrode materials such as conductive activated carbon. In contrast, in the present paper, we consider the use of the transition metals, and in particular copper, for aqueous-based, non-flammable, supercapacitors.

Carbonaceous materials are popular because they can be prepared with exceedingly high specific surface area, are cheap, light and chemically stable, and have sufficient electrical conductivity. In contrast, pseudocapacitors, which achieve their capacitance through a combination of DLC in conjunction with sequenced redox reactions on the surface of electrodes, are based on metallic electrode materials such as RuO_2 [7], MnO_2 [8], SnO_2 [9], NiO_x [10], Co_3O_4 [11], Cu_2O [12] and Mn_3O_4/graphene nanocomposites [13]. The electrical conductivity of these latter materials is much greater than that of most common forms of carbon, a factor that can justify their use in some applications.

One issue with all supercapacitors is their potential electrical inefficiency due to ohmic losses during charge and discharge [6, 14]. This is an important factor to consider in devices which need to undergo rapid and frequent cycling with the added constraint of maximum conservation of electrical energy. The peak electrical power, P_{peak}, that can be drawn from a supercapacitor in the process of discharging it from V_0 to $1/2V_0$ is given by Eq. (1) [6]

$$P_{peak} = \frac{9}{16}(1 - E_F)\frac{V_0^2}{R} \quad (1)$$

where E_F is the discharge efficiency, V_0 the initial discharge voltage and R the internal resistance. Clearly, if a high electrical efficiency is needed, then the amount of power that can be drawn is limited. In addition, a high internal resistance is undesirable. Unfortunately both the electrodes and organic electrolytes normally used for supercapacitors have relatively high electrical resistivity. These factors may handicap the performance of supercapacitors in some applications.

Improved efficiency, albeit it at a lower voltage, can be achieved by using an aqueous electrolyte, which will generally have a much lower resistivity [2, 3]. Similarly, the use of nanoporous transition metal electrodes could reduce energy loss due to their superior electrical conductivity relative to carbonaceous electrodes [15]. A supercapacitor based on these principles could be useful in applications requiring maximum volumetric power density and minimum electrical losses. Note, however, that the total energy stored is proportional to V^2 and the voltage that can be sustained across an aqueous electrolyte is limited to about 1 V (in contrast to the ~ 2.7 V that is possible with an organic electrolyte [3]). Therefore, the rational use of a supercapacitor with transition metal electrodes is confined to applications in which energy *efficiency* over repeated cycling is considered more important than total amount of energy delivered (this constraint does not apply to metallic pseudocapacitive systems).

Most of the transition metals will displace hydrogen from water and therefore are not suitable for use as metallic electrodes in aqueous supercapacitors. There are a few useful exceptions, however, especially the more noble elements such as Ag [16], Au [17] and Pt [18]. Nanosponges of the slightly less noble elements Ni [19] and Cu [20] can also be stable in water under certain conditions. (Note that IUPAC recommends [21] that the adjective *mesoporous* not *nanoporous* is appropriate for the pore-sizes involved. However, in keeping with usage in recent literature we will use *nanoporous* here.) There is quite an extensive literature on nanoporous gold (see, for example, the book edited by Wittstock [22]), and it has been occasionally considered as a potential electrode for supercapacitors [15, 23, 24] or for electroanalytical applications [25] because it is the most stable of the metallic elements with respect to oxidation. Unfortunately, gold nanosponges are too expensive for widespread application.

Here we investigate the feasibility of a supercapacitor based on *bulk* nanoporous copper (NPC). Compared to gold, copper has a much lower cost, a lower density (8.96 vs. 18.9 g cm^{-3}), about the same electrical conductivity (58.4 vs. 44.0 MS m^{-1} @ 25 °C), and a higher elastic modulus (110 vs. 77 GPa); however, its reduction potential is considerably less than that of gold (+ 0.34 vs. + 1.69 V). The last factor is responsible for the inferior oxidation resistance of NPC relative to nanoporous Au. The tendency of copper to oxidize turns out to be an advantage, however, as Cu/Cu oxide electrodes provide a pseudocapacitive capability [12, 26–28] through the reversible action of the reaction $Cu_2O + 2OH^- \rightarrow 2CuO + H_2O + 2e^-$.

As with other nano- or mesoporous metallic sponges, NPC can be conveniently prepared by de-alloying of a precursor alloy between itself and some more active metallic element, such as Al. A variety of etchants, both acidic and alkaline [29–34], have been used. The process is inspired by Raney's 1927 patent to produce nanoporous Ni catalyst [35] and indeed, NPC is sometimes described as 'Raney copper' [36]. Generally speaking, successful synthesis of a nanoporous metallic sponge by this route requires (i) a bimetallic precursor alloy with a large difference electrochemical reduction potential between noble element and active element, (ii) an alloy composition in which the mole fraction of the active element is above the 'parting limit' of about 0.6 but below about 0.9, (iii) that the surface diffusion during de-alloying surpasses the threshold diffusivity (about 10^{-14} cm^2 s^{-1}) required to form a backbone of the noble element, and (iv) that the starting alloy must be primarily homogenous and ideally stress free [20, 37–39]. Nanoporous metal sponges fabricated according to these criteria will consist of a three dimensional, bi-continuous architectures of interpenetrating ligaments and channels. Naturally, such a structure will have an elevated surface area per unit volume compared to bulk material.

Due to the advantageous properties offered by copper, there is currently considerable interest in the use of it in supercapacitors and, if copper oxide is also formed, in pseudocapacitors. Among the more recent reports, Mirzaee and Dehghanian report a thin-film Cu sponge supercapacitor prepared by electrodeposition [40], Yue et al. describe a Cu supercapacitor prepared by de-alloying a metallic glass precursor [41], while Du et al. used electrochemical oxidation to synthesize a supercapacitor electrode consisting of Cu_xO on nanoporous Cu [26]. The present work, however, differs in that it describes how bulk nanoporous copper sponge prepared by de-alloying bulk Cu–Al ingots can be used in a supercapacitor device.

Materials and methods

Preparation of $Cu_{17.5}Al_{82.5}$ (at.%) alloy

Ingots of alloy with masses of the order of 15.5 g (7.74 g each electrode) were fabricated by melting copper (Syneco A Grade, 99.999% purity) and aluminum pellets (Sigma Aldrich, 99.99% purity) in an alumina crucible under a protective flux of NaCl-KCl (50:50 molar ratio) and within a protective atmosphere produced by packing the crucible in a bed of charcoal and Al to scavenge O_2 (Fig. 1). A temperature of 800 °C was applied, with the entire process taking about 1.5 h. The $Cu_{17.5}Al_{82.5}$ composition corresponds to a eutectic in this system (Fig. 2).

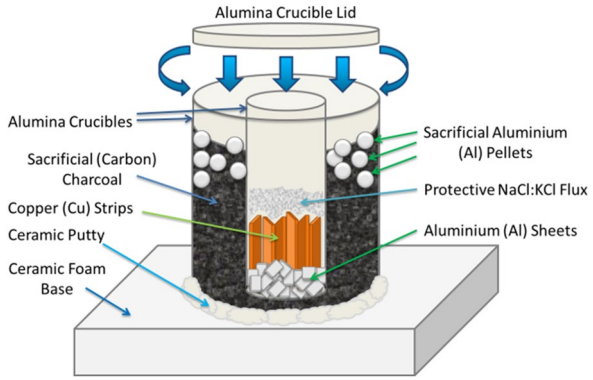

Figure 1: Schematic illustration of melting technique used to prepare small quantities of Cu–Al alloy.

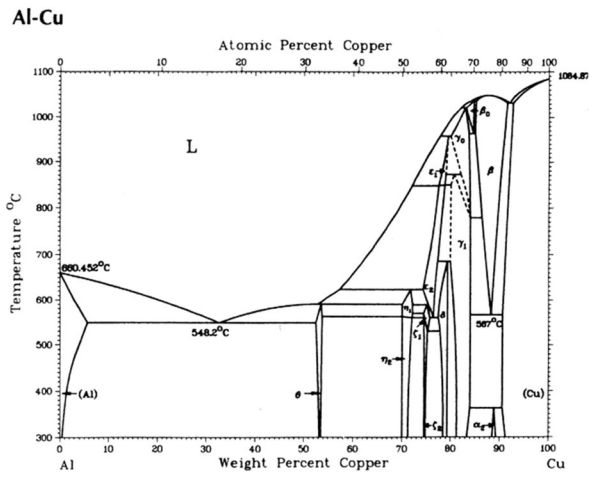

Figure 2: Equilibrium phase diagram of Cu–Al system showing eutectic point. (reproduced from Murray et al. [42] by permission of ASM International).

Fabrication of nanoporous copper electrodes

The ingots were cut in half using an abrasive ceramic cutting wheel and each half then cold-mounted into acrylic resin (Struers Acryfix Powder and Liquid (2:1 volume ratio)) with the cut face exposed. Once the acrylic resin was set, holes were drilled into the back of each electrode, electrical leads inserted, and then the contact area was sealed with acrylic resin. Nanoporous sponge was then allowed to form on the exposed faces of the electrodes by de-alloying of the Al using 5 M NaOH. De-alloying was continued for 96 h with the NaOH periodically refreshed every 24 h. The amount of aluminum removed from the master alloy was estimated by monitoring the current passed during de-alloying between an electrode and a solid piece of copper, and applying Faraday's Law. Clearly, when this current reaches zero, the copper sponge has no accessible metallic aluminum remaining.

Topographical and EDS analysis of NPC sponges

Topographical analysis of the NPC sponges was carried out using a Zeiss Supra 55VP FEG SEM to observe the extent of porosity and to estimate the ligament diameters. IMAGEJ (https://imagej.net) was used to make the measurements. One hundred ligaments were measured in a direction judged to be characteristic of their diameter. Quantitative analysis using software INCA Analyzer was conducted to analyze the atomic/weight percent composition prior to de-alloying and after de-alloying for the master Cu–Al alloy. Acquisition of EDS results relied upon calibrating with standardized copper first ($\lambda = 1.5418$ Å for Cu Kα). Results are provided in Table 1.

The grain size of the Cu in the sponge was estimated by applying a Scherrer analysis to X-ray diffraction patterns obtained at the Australian Synchrotron. A wavelength of 0.05896 nm was used (refined on NIST standard LaB_6 660b). The full-width half-maximum of the Cu 111, 002, 022 and 113 peaks was found by fitting a PseudoVoigt peak to the data using FitYK [43] and the results averaged. Instrument broadening at each value of 2θ was obtained using the LaB_6 standard. Pattern matching was performed using MATCH! (www.crystalimpact.

TABLE 1: Composition of electrodes (a) prior to and (b) after de-alloying, as measured by SEM EDS.

(a)						
Initial Cu–Al alloy	Cu (wt%)	Cu (wt%) ± σ error	Cu (at.%)	Al (wt%)	Al (wt%) ± σ error	Al (at.%)
N/A	33.15	0.83	17.39	66.85	0.83	82.61
	33.74	1.03	17.78	66.26	1.03	82.22
	33.18	0.81	17.41	66.82	0.81	82.59
(b)						
NaOH concentration (M)	Cu (wt%)	Cu (wt%) ± σ error	Cu (at.%)	Al (wt%)	Al (wt%) ± σ error	Al (at.%)
5.0	97.87	0.73	95.12	2.13	0.73	4.88
	97.81	0.83	94.99	2.19	0.83	5.01
	98.32	0.24	96.13	1.68	0.24	3.87

de). MATCH! was also used as the GUI through which FULLPROF (www.ill.eu/sites/fullprof/ index.html) was run for Rietveld refinement.

Brunauer–Emmett–Teller (BET) analysis of NPC sponges

Specific surface area of the NPC sponge electrodes was measured by BET analysis using a sample with a mass of 0.1885 g. Nitrogen adsorption/desorption measurements were carried out at a temperature of 77 K with a Micromeritics 3Flex Surface Characterization Analyzer. From this, a plot of Quantity Adsorbed ($cm^3\ g^{-1}$ STP) vs. relative pressure (P/P_0) was acquired.

Ostensible capacitance of NPC sponges

The ostensible capacitance of the device was measured by constructing a RC circuit which consisted of a DC power supply, an external resistor (R_e) of 1kΩ, a relay (H100SD12-1, to switch states), a transistor (BC 547, to drive the relay), an op amp (741 OA, amplifying the output potential) and a diode (IN4004, to control the direction of current flow). The circuit was prepared by connecting the electrodes, which were immersed in 0.1 M KNO_3, to the RC circuit (Fig. 3). The RC circuit was connected to a LabJack U3-HV A/D convertor which measured the voltage across the capacitor electrodes during the charging and discharging processes. Since there are two identical electrodes, and hence two capacitors, in series, the net capacitance of system is one half of either electrode on its own [2].

We will use the term 'ostensible capacitance' to characterize the electrical behavior of the composite device, defined as the apparent capacitance measured external to the device. This encompasses both the non-faradaic double-layer capacitance and any faradaic pseudocapacitance or other residual faradaic processes which might contribute to the flow of charge [15]. The ostensible capacitance is essentially the same as the so-called 'equivalent series capacitance' and is strictly speaking valid only for the specific charge/discharge cycle applied. (Here we apply a long period square wave to charge and discharge our device on the trailing edge of the square wave). This parameter is not necessarily identical to the true physical capacitance which must be independent of frequency or waveform. The ostensible capacitance can be estimated three ways. The first is to take the basic equation

$$i = C.\frac{\mathrm{d}V}{\mathrm{d}t} \tag{2}$$

and obtain an estimate of C from the current passed during the discharge. A numerical technique was used to estimate $\frac{\mathrm{d}V}{\mathrm{d}t}$. The second method was to modify the basic RC discharge equation ($V_c = V_0 e^{-\frac{t}{RC}}$, where R is the resistance) by adding (*i*) a time-varying capacitance $C = C_0 t^{C_1}$ and (*ii*) a small offset voltage, V_{off}, to account for residual galvanic effects (V_{galv}) and voltage drop due to the internal resistance (R_i) of the device. Let $R_{tot} = R_i + R_e$ be the total resistance of the circuit during discharge, then, after collecting terms and simplifying:

$$V(t) = \frac{V_{galv} + V_0 e^{\frac{-t}{R.C_0 t^{C_1}}}}{1 - \frac{R_i}{R_{tot}}} \tag{3}$$

where C_0 is the capacitance at the instant the discharge is initiated (i.e., $t = 0$) and C_1 an empirical coefficient. A variable value of 'C' can be used for devices that are not true dielectric or electrolytic capacitors, and represents an attempt to take faradaic phenomena into account [44]. The fit was determined by nonlinear optimization using FitYK [43]. A third method is to use the formula for discharge over a constant resistance, but taken over a moving window of, for example, 100 s:

$$C_t = \frac{t}{R.\ln\left(V_t/V_0\right)} = \frac{100}{R.\ln\left(V_t/V_{(t-100)}\right)} \tag{4}$$

The three approaches were found to provide broadly similar estimates of the capacitance.

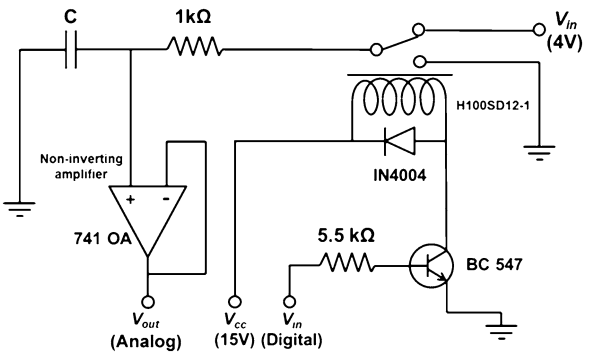

Figure 3: Circuit used to measure the ostensible capacitance of prototype device.

Results and discussion

The morphology of the copper sponges that we synthesized is shown in Fig. 4(a). The BET surface area was $11.9 \pm 0.1\ m^2\ g^{-1}$. After taking into account the greater density of Cu than carbon, it can be said that the material had roughly the same surface area *per unit volume* as a carbon of $45\ m^2 g^{-1}$. Application of the Scherrer equation to X-ray diffraction patterns collected on a synchrotron indicated that the grain size of the Cu in the freshly prepared sponge was 19 ± 4 nm, which may be compared to the ligament diameter of 51 ± 15 nm measured by SEM. The channels were of the order of 40 nm in diameter. To a first approximation the microstructure was therefore that of a symmetrical

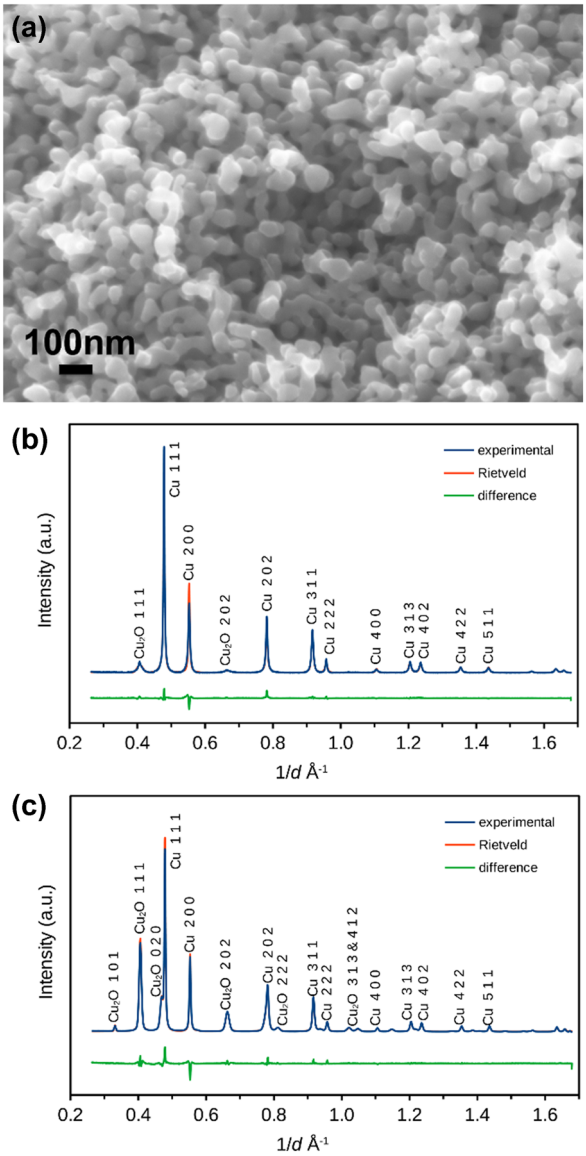

Figure 4: Nanoporous copper sponge prepared by de-alloying a Cu–Al eutectic alloy with 5 M NaOH for 96 h. (a) SEM image of freshly prepared sponge, (b) X-ray diffraction pattern of freshly prepared sponge showing presence of Cu and 13.3 wt% Cu_2O. (c) X-ray diffraction pattern of sponge heat treated for 30 min at 700 °C showing presence of Cu and 51 wt% Cu_2O.

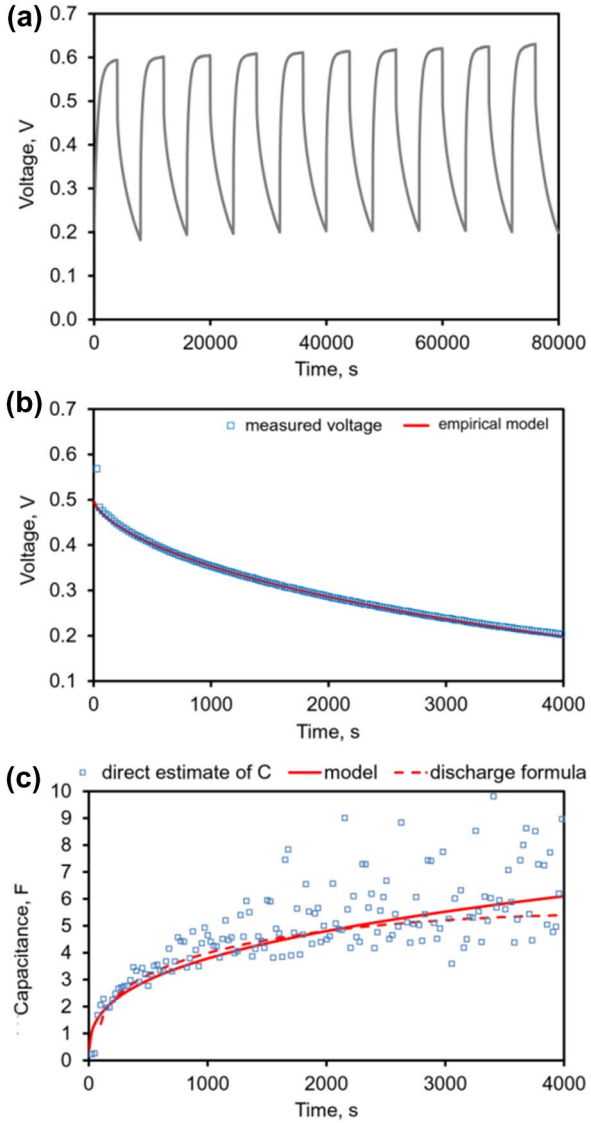

Figure 5: Performance of prototype metal sponge supercapacitor. (a) Voltage vs. time plot for a sequence of ten charge–discharge cycles. (b) voltage vs. time for 5th discharge showing fitted model and experimental data, (c) capacitance vs. time for 5th discharge with fitted values shown as solid line, values obtained from $C = i.\left(\frac{dV}{dt}\right)^{-1}$ as symbols and estimate from Eq. (4) as dashed line.

bi-continuous sponge. After 30 min of heat treatment at 700 °C, the Scherrer grain size was 23 ± 7 nm, showing that, within statistical error, the grains did not grow during the heat treatment. As synthesized, the copper ligaments were coated with a thin layer of Cu_2O which Rietveld refinement ($R_p = 4.6$) indicated comprised 13.3 ± 0.3 wt% of the sample [Fig. 4(b)]. This structure was surprisingly resistant to thermally-induced coarsening. A 30 min heat treatment at 700 °C in air caused significant further formation of Cu_2O to 51 ± 0.4 wt% ($R_p = 6.0$) [Fig. 4(c)]. We ascribe the lack of grain growth to the fact that further thickening of the ligaments was constrained by the surface coating of Cu_2O. Presumably the grains of Cu annealed into a stable 'bamboo-like' structure within the ligaments.

The capacitance of the sponges was experimentally determined by evaluating a sequence of square wave charge/discharge cycles of a symmetrical electrode system in 0.1 M KNO_3 aqueous electrolyte [Fig. 5(a)]. The form of the discharge curve (i.e., it is not a simple exponential decay) indicate that there is a variable aspect to the capacitance, as indeed is often the case for supercapacitors [6, 14, 44]. Specifically, in the present devices, the ostensible capacitance begins low and increases

with time during the discharge. There are two possible explanations for this. The first is that mass transfer of ions must occur in order for charge to flow, and therefore ions (charge) located in the more accessible, larger channels move first, followed later by that in deeper, more tortuous channels, so that the ostensible capacitance becomes a function of discharge voltage, time and current [6, 14]. A second and additional reason is that the Cu_2O coating on the NPC may be exerting a degree of pseudocapacitance by taking part in a Cu^{2+}/Cu^{1+} redox reaction [12]. The three approaches described in the Experimental Section were applied to estimate capacitance, and the results are shown in Fig. 5(b) and (c) for the 5th discharge cycle, which was a typical example. The discharge begins with an initial sharp drop in device voltage which is associated with the ostensible capacitance rising from about 0.3 F to 1 F for the device. Thereafter, the capacitance increases monotonically, passing a value of 4.5 F at V/V_o of 0.5 and reaching of the order of 6 F at V/V_0 of 0.3.

Further insight can be gained by comparing the discharge behavior of the sponge electrodes before and after de-alloying, and to that of copper sheet electrolytes of similar macroscopic surface area [Fig. 6(a)]. The discharge curves of the un-de-alloyed electrodes show little capacitance (only 1×10^{-2} F or $\sim 4 \times 10^{-4}$ F cm^{-2}). This a consequence of the relatively low surface area of the cast electrodes combined with the normal double-layer capacitance of the electrolyte. Greater capacitance ($\sim 8 \times 10^{-2}$ F, equivalent to 3.5×10^{-3} F cm^{-2}) and a degree of pseudocapacitance is shown by ordinary copper sheets. In contrast, the particular copper sponge electrodes shown in this figure have a capacitance of 3.5 ± 0.1 F, or ~ 0.15 F cm^{-2}. A plot of $\ln(V/V_0)$, Fig. 6(b), can be used to further unpack the deviation from purely capacitive behavior [44]. It is clear that the voltage decline on the copper electrodes during a discharge goes through two regimes, an initial relatively rapid decline corresponding to a relatively low equivalent circuit capacitance, followed by a linear (in $\ln(V/V_o)$ coordinates) regime where more typical capacitance behavior applies and the value of the ostensible C is much larger. According to Lewandowski et al., it is likely that the phenomena of a faradaic reaction, charge redistribution or current leakage could be operating during this initial phase in some kinds of supercapacitor. The effect of current density in the pseudocapacitive regime was also assessed by varying the charging potential from 0.4 to 1.4 V. Since the charging current decreases rapidly during charging at a constant voltage due to polarization at the surfaces of the electrode, we have plotted the data in Fig. 6(c) against the current density at 100 s into the charge cycle in order to ensure a stable comparison. The capacitance was calculated for the region between 100 and 250 s of each discharge cycle, a time range which lies in the pseudocapacitive part of a discharge cycle. It is evident that there is only a slight decrease in capacitance with increase in current density.

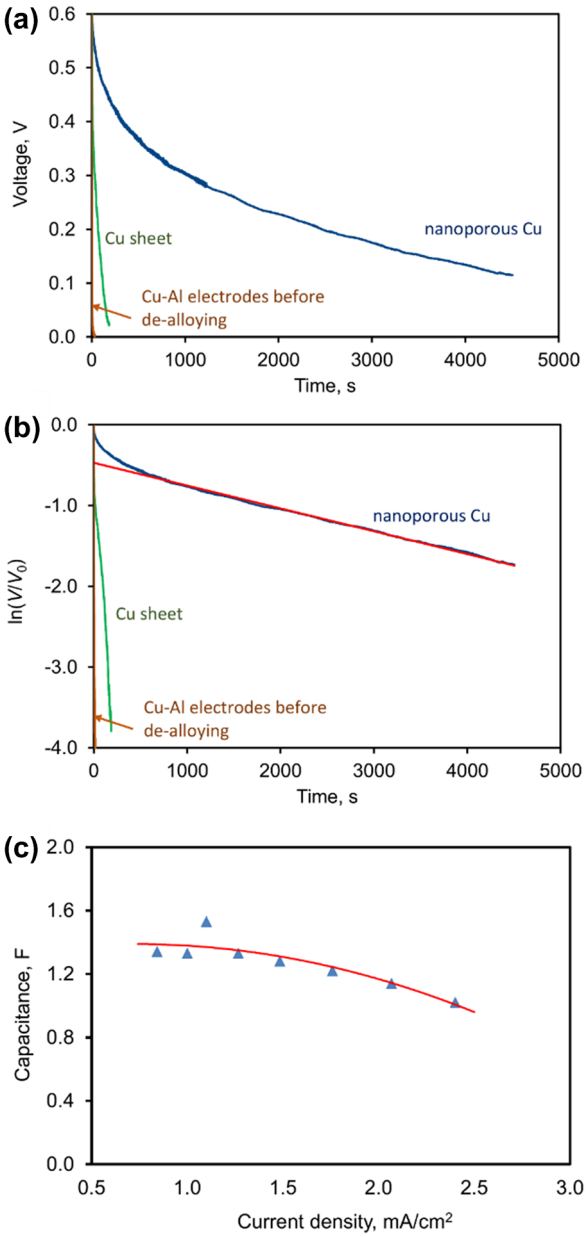

Figure 6: Comparison of copper sponge electrodes to non-sponge electrodes. (a) Discharge curves for a pair of Cu–Al electrodes before de-alloying, and after de-alloying. The discharge of a pair of Cu sheet electrodes of the same nominal surface area as the un-de-alloyed Cu–Al electrodes is also shown. (b). The deviation of the device from purely capacitive behavior is most evident during the early stages of the discharge cycle (0 to 1000 s). The superimposed red line (fitted between 1000 to 4000 s) illustrates purely capacitive behavior. (c) The effect of current density on the ostensible capacitance in the pseudocapacitive region, measured between 100 and 250 s into the discharge.

At this stage the present work is not able to differentiate between which of the two groups of phenomena (delayed mass transfer of ions from deeply buried channels, or the non-capacitive factors mentioned by Lewandowski et al.) are responsible for the variation in ostensible capacitance in this transition metal prototype device but the data for the copper

sheet strongly suggests that it is pseudocapacitance. Cyclic voltammetry measurements on this system would potentially resolve these questions and is planned for future work.

Since the electrodes were deliberately not completely dealloyed (in order that their back faces remained solid enough to attach leads), the amount of sponge in them cannot be measured directly. However, from the current generated during dealloying and using Faraday's law, it can be estimated that about 3.6 g of Al was removed from each electrode during sponge formation (out of a total of 5.16 g Al per electrode) to leave about 2.6 g of Cu sponge. Also, assuming that the original dimensions of the alloy were retained, this must equate to a sponge volume of 2.20 cm^3. Therefore, the capacitance of the prototype device was of the order of 2.3 F g^{-1} or 2.7 F cm^{-3} at 6 F, reducing to 1.6 F g^{-1} and 1.8 F cm^{-3} at 4 F. These results are inferior to those previously reported for by Deng et al. for their Cu_2O/Ni system [12] but it should be noted our results are for a real power output and not estimated from cyclic voltammetry. In addition, these are bulk (i.e., gram scale) materials and their capacitance per gram cannot be compared directly to that of the micro- or nanoscale thin films described in some other reports. Nevertheless, a metal sponge device will always rank poorly relative to a carbon one in a gravimetric comparison. In contrast, the volumetric comparison is more encouraging, although we stress again that the rational application of such a device must surely only be in applications where a very low internal resistance and high fire safety is mandated. The cyclic energy efficiency of these prototype capacitors is currently low due to overcharging and other sources of loss and, in addition, long life cyclic tests of thousands of charge–discharge cycles are still needed to verify the long-term stability of the material. Nevertheless, the results are very promising and illustrate some of the possibilities for a very low cost aqueous supercapacitor that can operate under atmospheric conditions. It is also probable that the present device can be further optimized by elimination of non-participating electrode material and by boosting the pseudocapacitive aspect from the Cu_2O surface coating.

Conclusions

We have shown how prototype nanoporous copper sponges with an open cell, three dimensional, bi-continuous interpenetrating ligament/channel structure can serve as the electrode in a conceptual double-layer supercapacitor with an aqueous electrolyte. The advantages of such a device are that it is low in cost, very safe, not flammable, can operate under atmospheric conditions, and will have very low ohmic losses on cycling. The main disadvantage is that the operating voltage is restricted by the breakdown potential of water and hence the device will have inferior energy density compared to devices that use organic electrolytes. The capacitance obtained from the simple prototypical device was about 2 F per gram of Cu, and increased with the degree of discharge of the device. Geometric optimizations of the device could very easily be made in order to increase the electrode surface area, for example, the NPC could be deposited onto flexible sheets which could then be assembled into a sandwich arrangement with a porous spacer and rolled up. In addition, the pseudocapacitive faradaic behavior of the sponge could be developed further.

Acknowledgments

The authors thank ANSTO for providing access to the Powder Diffraction beamline at the Australian Synchrotron. The technical assistance of Dr Justin Kimpton is acknowledged.

Funding

Open Access funding enabled and organized by CAUL and its Member Institutions.

Data availability

The data that support the findings of this study are available from the corresponding author upon reasonable request.

Declarations

Conflict of interest On behalf of all authors, the corresponding author states that there is no conflict of interest.

Open Access

References

1. A.S. Aricò, P. Bruce, B. Scrosati, J.M. Tarascon, W. Van Schalkwijk, Nanostructured materials for advanced energy conversion and storage devices. Nat. Mater. **4**(5), 366 (2005)
2. C. Liu, F. Li, L.-P. Ma, H.-M. Cheng, Advanced materials for energy storage. Adv. Mater. **22**(8), E28 (2010)

3. M. Winter, R.J. Brodd, What are batteries, fuel cells, and supercapacitors? Chem. Rev. **104**(10), 4245 (2004)
4. B. Conway, *Electrochemical Supercapacitors: Scientific Fundamentals and Technological Applications* (Kluwer Academic/Plenum, New York, 1999)
5. P. Simon, Y. Gogotsi, Materials for electrochemical capacitors. Nat. Mater. **7**(11), 845 (2008)
6. A. Burke, Ultracapacitors: why, how, and where is the technology? J. Power Sources. **91**, 37 (2000)
7. R.-R. Bi, X.-L. Wu, F.-F. Cao, L.-Y. Jiang, Y.-G. Guo, L.-J. Wan, Highly dispersed RuO_2 nanoparticles on carbon nanotubes: facile synthesis and enhanced supercapacitance performance. J. Phys. Chem. C. **114**(6), 2448 (2010)
8. Z. Yu, B. Duong, D. Abbitt, J. Thomas, Highly ordered MnO_2 nanopillars for enhanced supercapacitor performance. Adv. Mater. **25**(24), 3302 (2013)
9. R.K. Selvan, I. Perelshtein, N. Perkas, A. Gedanken, Synthesis of hexagonal-shaped SnO_2 nanocrystals and SnO_2@C nanocomposites for electrochemical redox supercapacitors. J. Phys. Chem. C. **112**(6), 1825 (2008)
10. K.W. Nam, K.B. Kim, A study of the preparation of NiOx electrode via electrochemical route for supercapacitor applications and their charge storage mechanism. J. Electrochem. Soc. **149**(3), A346 (2002)
11. G. Wang, H. Liu, J. Horvat, B. Wang, S. Qiao, J. Park, H. Ahn, Highly ordered mesoporous cobalt oxide nanostructures: synthesis, characterisation, magnetic properties, and applications for electrochemical energy devices. Chem. Eur. J. **16**(36), 11020 (2010)
12. M.-J. Deng, C.-Z. Song, P.-J. Ho, C.-C. Wang, J.-M. Chen, K.-T. Lu, Three-dimensionally ordered macroporous Cu_2O/Ni inverse opal electrodes for electrochemical supercapacitors. Phys. Chem. Chem. Phys. **15**, 7479 (2013)
13. B. Wang, J. Park, C. Wang, H. Ahn, G. Wang, Mn_3O_4 nanoparticles embedded into graphene nanosheets: Preparation, characterization, and electrochemical properties for supercapacitors. Electrochim. Acta. **55**(22), 6812 (2010)
14. B.E. Conway, W.G. Pell, Power limitations of supercapacitor operation associated with resistance and capacitance distribution in porous electrode devices. J. Power Sources. **105**, 169 (2002)
15. M.B. Cortie, A.I. Maaroof, G.B. Smith, Electrochemical capacitance of mesoporous gold. Gold Bull. **38**(1), 15 (2005)
16. H. Ji, X. Wang, C. Zhao, C. Zhang, J. Xu, Z. Zhang, Formation, control and functionalization of nanoporous silver through changing dealloying media and elemental doping. Cryst. Eng. Comm. **13**, 2617 (2011)
17. J. Erlebacher, M.J. Aziz, A. Karma, N. Dimitrov, K. Sieradzki, Evolution of nanoporosity in dealloying. Nature **410**, 450 (2001)
18. S. Supansomboon, A. Porkovich, A. Dowd, M.D. Arnold, M.B. Cortie, Effect of precursor stoichiometry on the morphology of nanoporous platinum sponges. ACS Appl. Mater. Interfaces. **6**(12), 9411 (2014)
19. Y. Li, Y. Liu, Y. Yang, F. Yu, J. Liu, H. Song, J. Liu, H. Tang, B.C. Ye, Z. Sun, Novel electrochemical sensing platform based on a molecularly imprinted polymer decorated 3D nanoporous nickel skeleton for ultrasensitive and selective determination of metronidazole. ACS Appl. Mater. Interfaces. **7**(28), 15479 (2015)
20. J.R. Hayes, A.M. Hodge, J. Biener, A.V. Hamza, K. Sieradzki, Monolithic nanoporous copper by dealloying Mn-Cu. J. Mater. Res. **21**(10), 2611 (2006)
21. A.D. McNaught, A. Wilkinson, *Compendium of Chemical Terminology* (Blackwell Scientific Publications, New York, 1997)
22. A. Wittstock, J. Biener, J. Erlebacher, M. Bäumer, *Nanoporous Gold: From an Ancient Technology to a High-tech Material* (Royal Society of Chemistry Publishing, Cambridge, 2012)
23. X.Y. Lang, H.T. Yuan, Y. Iwasa, M.W. Chen, Three-dimensional nanoporous gold for electrochemical supercapacitors. Scr. Mater. **64**(9), 923 (2011)
24. X. Lang, L. Zhang, T. Fujita, Y. Ding, M. Chen, Three-dimensional bicontinuous nanoporous Au/polyaniline hybrid films for high-performance electrochemical supercapacitors. J. Power Sources. **197**, 325 (2012)
25. R. Jurczakowski, C. Hitz, A. Lasia, Impedance of porous gold electrodes in the presence of electroactive species. J. Electroanal. Chem. **582**(1–2), 85 (2005)
26. X. Du, C. Xia, Q. Li, X. Wang, T. Yang, F. Yin, Facile fabrication of Cu_xO composite nanoarray on nanoporous copper as supercapacitor electrode. Mater. Lett. **233**, 170 (2018)
27. Z. Endut, M. Hamdi, W.J. Basirun, Pseudocapacitive performance of vertical copper oxide nanoflakes. Thin Sol. Films. **528**, 213 (2013)
28. L. Xu, J. Li, H. Sun, X. Guo, J. Xu, H. Zhang, X. Zhang, In situ growth of Cu_2O/CuO nanosheets on Cu coating carbon cloths as a binder-free electrode for asymmetric supercapacitors. Front. Chem. **7**, article 420 (2019).
29. Y. Wang, Y. Wang, C. Zhang, T. Kou, Z. Zhang, Tuning the ligament/channel size of nanoporous copper by temperature control. CrystEngComm **14**(24), 8352 (2012)
30. M. Li, Y. Zhou, H. Geng, Fabrication of nanoporous copper ribbons by dealloying of Al-Cu alloys. J. Porous Mater. **19**(5), 791 (2012)
31. I.C. Cheng, A.M. Hodge, Morphology, oxidation, and mechanical behavior of nanoporous Cu foams. Adv. Eng. Mater. **14**(4), 219 (2012)
32. W. Liu, S. Zhang, N. Li, J. Zheng, S. An, G. Li, Influence of dealloying solution on the microstructure of monolithic nanoporous copper through chemical dealloying of Al 30 at.% Cu alloy. Int. J. Electrochem. Sci. **7**, 7993 (2012)
33. C. Zhao, X. Wang, Z. Qi, H. Ji, Z. Zhang, On the electrochemical dealloying of Mg–Cu alloys in a NaCl aqueous solution. Corros. Sci. **52**(12), 3962 (2010)
34. Z. Qi, C. Zhao, X. Wang, J. Lin, W. Shao, Z. Zhang, X. Bian, Formation and characterization of monolithic nanoporous

copper by chemical dealloying of Al–Cu alloys. J. Phys. Chem. C. **113**(16), 6694 (2009)
35. R.M. Raney, Method of producing finely-divided nickel. US Patents 1,628,190 (1927).
36. J.R. Mellor, N.J. Coville, S.H. Durbach, R.G. Copperthwaite, Acid leached Raney copper catalysts for the water–gas shift reaction. Appl. Catal. A. **171**(2), 273 (1998)
37. L.-Y. Chen, J.-S. Yu, T. Fujita, M.-W. Chen, Nanoporous copper with tunable nanoporosity for SERS applications. Adv. Funct. Mater. **19**(8), 1221 (2009)
38. J. Erlebacher, An atomistic description of dealloying - porosity evolution, the critical potential, and rate-limiting behavior. J. Electrochem. Soc. **151**(10), C614 (2004)
39. Z.H. Zhang, Y. Wang, Z. Qi, W.H. Zhang, J.Y. Qin, J. Frenzel, Generalized fabrication of nanoporous metals (Au, Pd, Pt, Ag, and Cu) through chemical dealloying. J. Phys. Chem. C. **113**(29), 12629 (2009)
40. M. Mirzaee, C. Dehghanian, Synthesis of nanoporous copper foam-applied current collector electrode for supercapacitor. J. Iran. Chem. Soc. **16**, 283 (2019)
41. X. Yue, R. Hu, J. Qi, Y. Sui, Y. He, Q. Meng, F. Wei, Y. Ren, Y. Zhao, Three-dimensional nanoporous copper with tunable structure prepared by dealloying titanium–copper–cobalt metallic glasses for supercapacitors. Micro Nano Lett. **15**(5), 283 (2020)
42. J.L. Murray, *Alloy Phase Diagrams* (ASM Materials International, Materials Park, 2002)
43. M. Wojdyr, Fityk : a general-purpose peak fitting program. J. Appl. Cryst. **43**, 1126 (2010)
44. A. Lewandowski, P. Jakobczyk, M. Galinski, M. Biegun, Self-discharge of electrochemical double layer capacitors. Phys. Chem. Chem. Phys. **15**, 8692 (2013)